This is a repository copy of *Low Order Model for the Dynamics of Bi-Stable Composite Plates*.

Low order model for the dynamics of bi-stable composite plates

Andres F. Arrieta*, Gottfried Spelsberg-Korspeter, Peter Hagedorn

System Reliability and Machine Acoustics, Dynamics and Vibrations Group
Technische Universität Darmstadt, LOEWE-Zentrum AdRIA, Darmstadt, 64289
Germany

Simon A. Neild, David J. Wagg

Department of Mechanical Engineering, University of Bristol, Bristol, U.K, BS8 1TR

Abstract

This paper presents the derivation and validation of a low order model for the nonlinear dynamics of cross-ply bi-stable composite plates focusing on the response of one stable state. The Rayleigh-Ritz method is used to solve the associated linear problem to obtain valuable theoretical insight into how to formulate an approximate nonlinear dynamic model. This allows us to follow a Galerkin approach projecting the solution of the nonlinear problem onto the mode shapes of the linear problem. The order of the nonlinear model is reduced using theoretical results from the linear solution yielding the low order model. The dynamic response of a bi-stable plate specimen is studied to simplify further the model by only keeping the nonlinear terms leading to observed oscillations. Simulations for the dynamic response using the derived model are presented showing excellent agreement with the exper-

---

*Corresponding author. Tel.:+4961517058324
Email address: andres.arrieta@dyn.tu-darmstadt.de (Andres F. Arrieta)

imentally observed behaviour. Furthermore deflection shapes are measured and compared to the calculated mode shapes, showing good agreement.

Key words: Bi-stable composites, Morphing structures, Low order modelling, Mode shapes

---

1. Introduction

Structures made from composite laminates are becoming increasingly important in a wide variety of applications including adaptive structures. Promising developments in this field relate to curved composite laminates which have multiple statically stable shapes [1]. These shapes result from an unsymmetric stacking sequence leading to asymmetric residual thermal stresses being induced during the curing process [2]. The transition between stable states is achieved by a snap-through mechanism which is strongly non-linear in nature [3]. Due to the property of multi-stability, these materials have been considered for use in a range of adaptive structures, particularly for morphing aerospace structures [4]. Recently, techniques to design the induced thermal stresses have allowed the production of a wide range of desired stable shapes [5], and aerospace applications using the designed morphing capabilities have been proposed [6].

Most of the studies on bi-stable composite laminates for morphing applications have focused on modelling the shape after the manufacturing process and their static characteristics [8, 9]. More specifically, these studies have focused on the identification of the stiffness characteristics [10, 11], and the static load required to induce snap-through [12, 13, 14]. However, the operating conditions of aerospace morphing applications will inevitably expose

these composite structures to high levels of dynamic excitation, for example in an aeroelastic environment. Potentially, dynamic excitations could induce undesired sudden jumps between stable states or even early fatigue failure to the structure. However, to date, very little work has been carried out to examine the dynamics of bi-stable composites. A theoretical study of the dynamics of snap-through in bi-stable composites has been conducted [15]. It compared a semi-analytical model for the deflection of bi-stable composites based on a strain energy approximation with Finite Element Analysis results, showing good agreement for the force required to trigger snap-through. Experimentally, high amplitude oscillations of a bi-stable plate, showing indications of chaotic oscillations across the snap-through region, have been presented [16]. In addition, the nonlinear dynamic response of a single stable state of a bi-stable composite plate was experimentally studied showing the response is dominated by 1/2 subharmonic oscillations [17].

The purpose of this paper is to derive a simple low order model for the dynamic response of cross-ply bi-stable composite plates confined to one stable state. Important dynamic features include subharmonic resonances, which have previously been observed in nonlinear vibration of flat composite plates [23], as they can lead to catastrophic failure of aerospace structures [24, 25], and the transverse vibration mode shapes. Modal frequencies and mode shapes are obtained following a Rayleigh-Ritz approach for the associated linear problem showing good agreement with experimental results. The Rayleigh-Ritz method has been employed to obtain analytical expressions for the mode shapes in previous theoretical studies on cylindrical isotropic shells [18], point supported plates [19], and orthotropic plates [20].

3

Experimental studies on the deflection of circular [21] and spherical isotropic plates [22] can be found in the literature. However, few studies comparing experimental deflection shapes to theoretical mode shapes were found in the literature [22]. To the knowledge of the authors no comparison between theoretical mode shapes and experimental deflection shapes for bi-stable composites has been presented. A good understanding of the deflection shape of such structures is paramount in the successful implementation of morphing and vibration suppression control for structures incorporating bi-stable composite. The nonlinear problem is approximated by following a Galerkin procedure projecting the solution onto the mode shapes of the linear problem obtaining a set of nonlinear modal equations. Theoretical observations from the linear solution show close agreement between the chosen shape functions and the mode shapes obtained for the associated linear problem allowing to reduce the order of the nonlinear model. An experimental characterisation is conducted for the linear and nonlinear response of a square carbon-fibre epoxy bi-stable plate $[0_4 - 90_4]_T$ test specimen showing very close agreement with the theoretical observations. In addition, this characterisation is used to retain the relevant nonlinear terms in the modal nonlinear equations of the low order model. A validation of the model is conducted by comparing simulated results for the key dynamic features of the response with experimental results.

The layout of the paper is as follows. In section 2, the Rayleigh-Ritz method is employed to obtain modal frequencies and mode shapes for the associated linear undamped shell vibration problem. Then, equations of motion for transverse displacement vibrations for bi-stable plates are derived

4

using Love's equations of motion for a shell including the von Kármán non-linearity in strain-displacement relations to account for geometric nonlinear-ities [26]. The Galerkin approach is followed to obtain a set of nonlinear ordinary differential equations using the shape functions employed in section 2 as a base for the expansion of the transverse displacement nonlinear solution. In section 3, the dynamic response of a test specimen is studied. Theoretical results are used to reduce the number of degrees-of-freedom and the required nonlinear terms to be kept in the equations to obtain a good low-order approximation for the dynamics of the plate, as described in section 4. In section 5, simulations for frequency response diagrams and displace-ment time series are conducted using the derived model showing good match with the experimental results. In section 6 of this paper, the mode shapes obtained in section 2 are compared to deflection shapes for the bi-stable plate specimen, showing good agreement. In addition, the deflection shapes for subharmonic oscillations are studied revealing a nonlinear behaviour in the spatial response. Finally, conclusions are presented and future research directions are discussed.

2. Model derivation

Classical nonlinear shell theory is employed to study the dynamics of bi-stable composites. Typical bi-stable composites are thin-walled shells having a small rise to span ratio, thus the principal curvatures are small as shown in Fig. 1. Practically, this implies that Cartesian coordinates x and y may be selected as the curvilinear coordinates for the middle surface of bi-stable composites, thus shallow shell theory is adopted [27]. In the derivation of
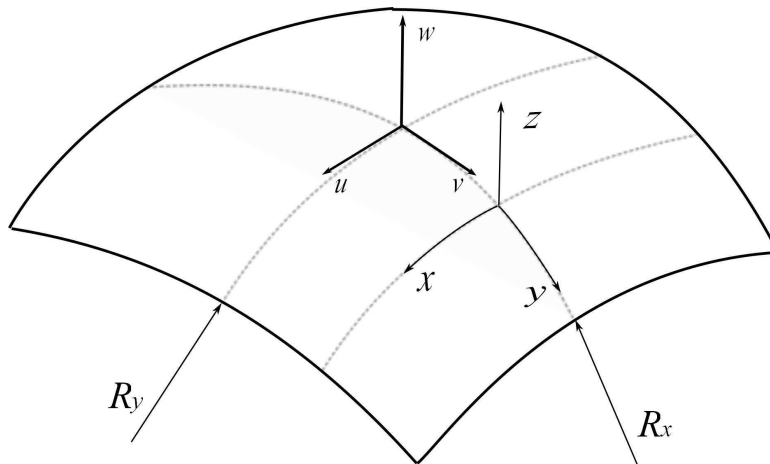
5

Figure 1: Curvilinear coordinates (x, y) and shell displacements $u(x, y, t)$, $y(x, y, t)$ and $w(x, y, t)$.

the model, first the associated linear problem is solved with the Rayleigh-Ritz method, allowing us to obtain mode shapes for the reduced nonlinear problem, as well as for comparison with experimentally measured deflection shapes. Secondly, a Galerkin procedure to approximate the solution of the nonlinear problem is conducted, using the same shape functions as for the Rayleigh-Ritz method to obtain nonlinear modal equations for the time response of cross-ply bi-stable composites.

2.1. Linear formulation

The Rayleigh-Ritz method is employed to solve the undamped linear problem [28]. These results provide valuable theoretical insight used to approximate the solution of the more complex nonlinear problem. Following a variational formulation, the total mechanical energy for an undamped, un-

symmetrically laminated shell is given by

$$\mathcal{L} = \mathcal{V} - \mathcal{T}, \tag{1}$$

where $\mathcal{L}$ is the Lagrangian of the system. The strain (potential) energy is written as

$$\mathcal{V}_s =$$

$$\int_{-L_x}^{L_x} \int_{-L_y}^{L_y} \left[N_{xx}\epsilon_{xx}^o + N_{yy}\epsilon_{yy}^o + N_{xy}\epsilon_{xy}^o + M_{xx}k_{xx} + M_{yy}k_{yy} + M_{xy}k_{xy} \right] dydx, \tag{2}$$

where N_{ij} and M_{ij} are the membrane forces and bending moments respectively, and L_x and L_y are the dimensions of the shell (see Fig. 1). The membrane and bending strains, ϵ^o and k respectively, are given by

$$\epsilon_{xx}^o = \frac{\partial u}{\partial x} + \frac{w}{R_x}, \tag{3a}$$

$$\epsilon_{yy}^o = \frac{\partial v}{\partial y} + \frac{w}{R_y}, \tag{3b}$$

$$\epsilon_{xy}^o = \frac{\partial u}{\partial y} + \frac{\partial v}{\partial x}, \tag{3c}$$

$$\tag{3d}$$

and

$$k_{xx} = -\frac{\partial^2 w}{\partial x^2}, \tag{4a}$$

$$k_{yy} = -\frac{\partial^2 w}{\partial y^2}, \tag{4b}$$

$$k_{xy} = -2\frac{\partial^2 w}{\partial x \partial y}. \tag{4c}$$

The membrane and bending strains are related to membrane forces and bending moments by the constitutive relations for an unsymetrically laminated

shallow composite shell [29], as

$$N_{xx} = A_{11}\epsilon_{xx}^o + A_{12}\epsilon_{yy} + B_{11}k_{xx},$$

$$N_{yy} = A_{21}\epsilon_{xx}^o + A_{22}\epsilon_{yy} + B_{22}k_{yy},$$

$$N_{xy} = A_{33}\epsilon_{xy}^o,$$

$$M_{xx} = B_{11}\epsilon_{xx}^o + D_{11}k_{xx} + D_{12}k_{yy},$$

$$M_{yy} = B_{22}\epsilon_{yy}^o + D_{21}k_{xx} + D_{22}k_{yy},$$

$$M_{xy} = D_{33}k_{xy}, \tag{5a}$$

where A_{ij}, B_{ij} and D_{ij} represent the membrane stiffnesses, coupling moduli and the bending stiffnesses of coordinate i acting on the direction j respectively, and $u(x,y,t)$, $v(x,y,t)$ and $w(x,y,t)$ are the displacements in the x, y and z coordinate directions. An additional term in the strain energy is introduced to account for an elastic support to which the bi-stable plate may be attached to, given by

$$\mathcal{V}_b = \frac{1}{2}\int_{-L_x}^{L_x}\int_{-L_y}^{L_y}\left[k_x u^2 + k_y v^2 + k_z w^2\right] dxdy, \tag{6}$$

where k_x, k_y and k_z are the elastic constants of the support in x, y and z directions [19]. The total strain energy is thus

$$\mathcal{V} = \mathcal{V}_s + \mathcal{V}_b. \tag{7}$$

The kinetic energy may be written as

$$\mathcal{T} = \frac{1}{2}\rho h\int_{-L_x}^{L_x}\int_{-L_y}^{L_y}\left[\dot{u}^2 + \dot{v}^2 + \dot{w}^2\right] dxdy, \tag{8}$$

where ρ is the density and h is the thickness of the shell, and the overdot $\dot{}$ symbol implies differentiation with respect to rime.

The types of shells studied herein have unrestricted edges, i.e. free boundary conditions. Thus, no restrictions are placed on the admissible functions (shape functions) for the Rayleigh-Ritz procedure, as no geometric boundary conditions need to be satisfied. The solutions for the displacements along each coordinate direction are represented by the expansions

$$
\begin{aligned}
u(x, y, t) &= \sum_{i=0}^{M} \sum_{j=0}^{N} U_{ij}(t) u_{ij}(x, y), \\
&= \sum_{i=0}^{I} \sum_{j=0}^{J} U_{ij}(t) \cos\left(\frac{\pi x i}{L_x}\right) \cos\left(\frac{\pi y j}{L_y}\right) \\
&+ \sum_{i=I+1}^{2I+1} \sum_{j=J+1}^{2J} U_{ij}(t) \cos\left(\frac{\pi x(i-(I+1))}{L_x}\right) \sin\left(\frac{\pi y(j-J)}{L_y}\right) \\
&+ \sum_{i=2I+2}^{3I+1} \sum_{j=2J+1}^{3J+1} U_{ij}(t) \sin\left(\frac{\pi x(i-(2I+1))}{L_x}\right) \cos\left(\frac{\pi y(j-(2J+1))}{L_y}\right) \\
&+ \sum_{i=3I+2}^{4I+1} \sum_{j=3J+2}^{4J+1} U_{ij}(t) \sin\left(\frac{\pi x(i-(3I+1))}{L_x}\right) \sin\left(\frac{\pi y(j-(3J+1))}{L_y}\right),
\end{aligned}
$$

$$(9)$$

9

$$v(x, y, t) = \sum_{i=0}^{M} \sum_{j=0}^{N} V_{ij}(t) v_{ij}(x, y),$$

$$= \sum_{i=0}^{I} \sum_{j=0}^{J} V_{ij}(t) \cos\left(\frac{\pi x i}{L_x}\right) \cos\left(\frac{\pi y j}{L_y}\right)$$

$$+ \sum_{i=I+1}^{2I+1} \sum_{j=J+1}^{2J} V_{ij}(t) \cos\left(\frac{\pi x(i - (I + 1))}{L_x}\right) \sin\left(\frac{\pi y(j - J)}{L_y}\right)$$

$$+ \sum_{i=2I+2}^{3I+1} \sum_{j=2J+1}^{3J+1} V_{ij}(t) \sin\left(\frac{\pi x(i - (2I + 1))}{L_x}\right) \cos\left(\frac{\pi y(j - (2J + 1))}{L_y}\right)$$

$$+ \sum_{i=3I+2}^{4I+1} \sum_{j=3J+2}^{4J+1} V_{ij}(t) \sin\left(\frac{\pi x(i - (3I + 1))}{L_x}\right) \sin\left(\frac{\pi y(j - (3J + 1))}{L_y}\right),$$

$$(10)$$

$$w(x, y, t) = \sum_{i=0}^{M} \sum_{j=0}^{N} W_{ij}(t) w_{ij}(x, y),$$

$$= \sum_{i=0}^{I} \sum_{j=0}^{J} W_{ij}(t) \cos\left(\frac{\pi x i}{L_x}\right) \cos\left(\frac{\pi y j}{L_y}\right)$$

$$+ \sum_{i=I+1}^{2I+1} \sum_{j=J+1}^{2J} W_{ij}(t) \cos\left(\frac{\pi x(i - (I + 1))}{L_x}\right) \sin\left(\frac{\pi y(j - J)}{L_y}\right)$$

$$+ \sum_{i=2I+2}^{3I+1} \sum_{j=2J+1}^{3J+1} W_{ij}(t) \sin\left(\frac{\pi x(i - (2I + 1))}{L_x}\right) \cos\left(\frac{\pi y(j - (2J + 1))}{L_y}\right)$$

$$+ \sum_{i=3I+2}^{4I+1} \sum_{j=3J+2}^{4J+1} W_{ij}(t) \sin\left(\frac{\pi x(i - (3I + 1))}{L_x}\right) \sin\left(\frac{\pi y(j - (3J + 1))}{L_y}\right),$$

$$(11)$$

where $U_{ij}(t)$, $V_{ij}(t)$ and $W_{ij}(t)$ are time response coefficients to be determined, $u_{ij}(x, y)$, $v_{ij}(x, y)$ and $w_{ij}(x, y)$ are the shape functions on each coordinate direction, and, $M = 4I + 2$ and $N = 4J + 2$ give the total number of shape

functions on each expansion as $M \times N$. Notice that the above given shape functions used to represent the displacements are all the possible non-zero combinations of sinusoidal functions. In addition to the constant term given by subscripts $i = 0$ $j = 0$, the two added terms in $M = 4I + 2$ and $N = 4J + 2$ account for the constants obtained from the cosine terms $\cos(0)$ multiplied by all the possible sine functions in each displacement direction.

Substituting Eqs. (9)-(11) into Eq. (1), and using Lagrange's equations [30]

$$\frac{d}{dt}\left(\frac{\partial \mathcal{L}}{\dot{q}_i}\right) - \frac{\partial \mathcal{L}}{q_i} = 0, \tag{12}$$

where the generalized coordinates q_i are the time responses forming the vector $\mathbf{q} = [U_{ij}(t), V_{ij}(t), W_{ij}(t)]^T$, the equations of motion for the linear problem are obtained by substituting $\mathbf{q} = \mathbf{k}e^{i\omega t}$ in Eq. (12), written as

$$\left(\mathbf{K} - \omega^2 \mathbf{M}\right)\mathbf{k} = 0. \tag{13}$$

The elements of the matrices $\mathbf{M}$ and $\mathbf{K}$ are given in Appendix A. Eigenvalues and eigenvectors of Eq. (13) are used for comparison to experimentally measured modal frequencies and deflection shapes. Furthermore, the eigenvalues of Eq. (13) serve as upper bounds for the modal frequencies in the design of bi-stable composites. Table 1 gives the modal frequencies of the first modes obtained from Eq. (13) for the case where a square bi-stable composite plate is not attached to an elastic support. The associated mode shapes (deformed shapes) are shown with respect to the undeformed shape (green) in Fig. 2. The first six modes shown are rigid body modes, three rotations with respect to the coordinate direction given as subscript, and three translations in each displacement direction, are shown in Figs. 2(a)-2(c) and Figs. 2(d)-2(f) respectively. These rigid body modes are important for the case where the shell

is attached to an elastic support, as is the case for any real specimen with free boundary conditions, for which the corresponding natural frequencies are non zero. Figs. 2(g)-2(l) show the first six flexible modes of the composite plate. Each are either symmetric (S) or antisymmetric (A) with respect to the (x,y) axes of the shell, thus the notation for the first out-of-plane mode having symmetry with respect to the x-direction and antisymmetry with respect to the y-direction is $(S, A)_1^w$. The corresponding mode shape for mode $(S, A)_1^w$ is $w_{(S,A)_1}$. The theoretical results obtained from Eq. (13) are further exploited in section 4 to obtain a low order model for the dynamics of bi-stable composites.

2.2. Nonlinear analysis

To study the nonlinear response of bi-stable composites the classical shallow shell nonlinear vibration theory is followed. This takes into account the effect due to the curvature and the stretching of the middle surface captured by the von-Kármán geometric nonlinearity in the strain-displacement relations [31], given by

$$\epsilon_{xx}^o = \frac{\partial u}{\partial x} + \frac{w}{R_x} + \frac{1}{2}\left(\frac{\partial w}{\partial x}\right)^2, \tag{14a}$$

$$\epsilon_{yy}^o = \frac{\partial v}{\partial y} + \frac{w}{R_y} + \frac{1}{2}\left(\frac{\partial w}{\partial y}\right)^2, \tag{14b}$$

$$\epsilon_{xy}^o = \frac{\partial u}{\partial y} + \frac{\partial v}{\partial x} + \frac{\partial w}{\partial x}\frac{\partial w}{\partial y}. \tag{14c}$$

The focus of the model is on the transverse deflection of bi-stable plates, thus the in-plane inertias are neglected in the derivation following the shallow shell theory [32]. The system of nonlinear partial differential equations is then simplified from three equations, one for each coordinate direction, to two

12

Mode	Modal Frequency $[Hz]$
$(0,0)_x$	0
$(0,0)_y$	0
$(0,0)_z$	0
$(S,S)_0^u$	0
$(S,S)_0^v$	0
$(S,S)_0^w$	0
$(A,A)_1^w$	19.8
$(S,S)_1^w$	45.7
$(A,S)_1^w$	61.6
$(S,S)_2^w$	128.1
$(S,A)_1^w$	130.9
$(S,A)_2^w$	138.8

Table 1: Modal frequencies for the first 12 modes. Notice that the first 6 modes are rigid body modes.

(a) $(0,0)_x(x,y)$ (b) $(0,0)_y(x,y)$ (c) $(0,0)_z(x,y)$ (d) $u_{(S,S)_0}(x,y)$

(e) $v_{(S,S)_0}(x,y)$ (f) $w_{(S,S)_0}(x,y)$ (g) $w_{(A,A)_1}(x,y)$ (h) $w_{(S,S)_1}(x,y)$

(i) $w_{(A,S)_1}(x,y)$ (j) $w_{(S,S)_2}(x,y)$ (k) $w_{(S,A)_1}(x,y)$ (l) $w_{(S,A)_2}(x,y)$
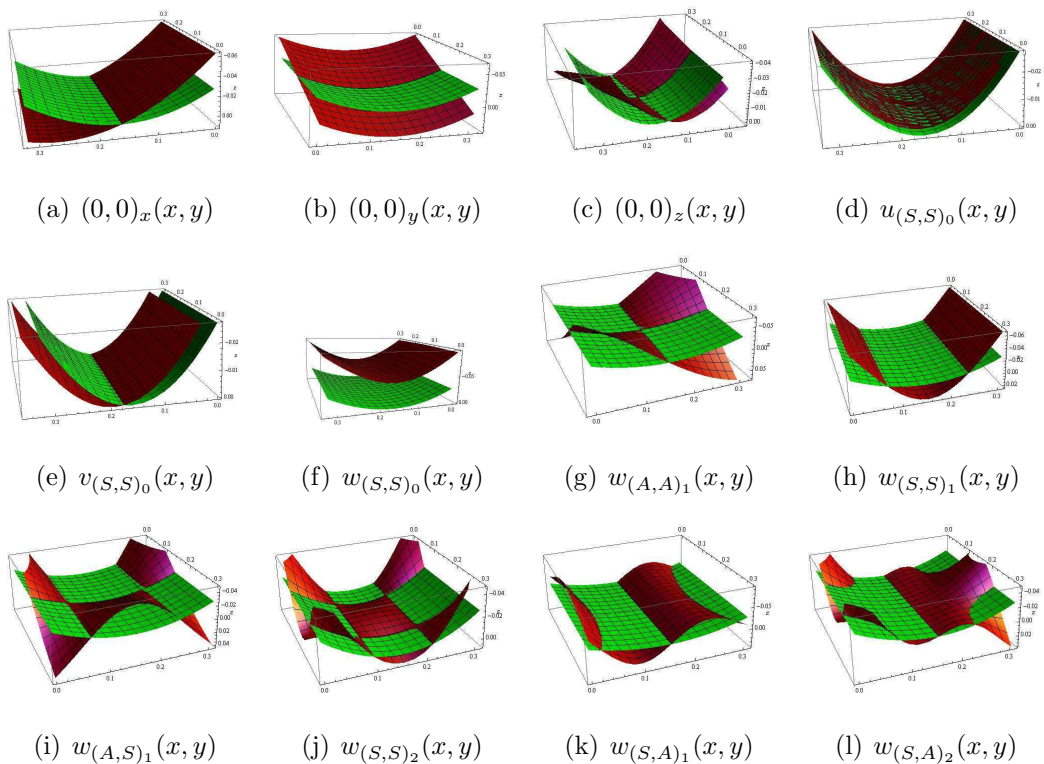
Figure 2: Mode shapes (deformed shapes) for the first 12 modes of a square cross-ply bi-stable composite plate with unsymmetrical stacking sequence obtained with Eq. (13). Figures 2(a)-2(c) show the rotational rigid body modes in the x-, y- and z-directions, and Figs. 2(d)-Fig. 2(f) show the translational rigid body modes in the x-, y- and z-directions. Flexural modes are shown in Figs. 2(g)-2(l) where the subscripts refer to the symmetry class and the modal number for each mode shape, e.g. $w_{(S,A)_1}$ refers to the first out-of-plane mode shape of the symmetric-antisymmetric symmetry class.

equations, one for the transverse displacement and one obtained from a compatibility equation. Based on the constitutive relations given in Eq. (5) and the above mentioned simplifications, the governing equation for the transverse displacement for a cross-ply unsymmetrically laminated bi-stable com-

14

posite is given by [35]

$$(D_{11} - P_{11}B_{11}^2)\frac{\partial^4 w}{\partial x^4} + 2(D_{12} + P_{12}B_{11}B_{22} + 2D_{33})\frac{\partial^4 w}{\partial x^2 \partial y^2} + (D_{22} - P_{22}B_{22}^2)\frac{\partial^4 w}{\partial y^4}$$

$$+\frac{1}{R_x}\frac{\partial^2 \phi}{\partial y^2} + \frac{1}{R_y}\frac{\partial^2 \phi}{\partial x^2} - \frac{\partial^2 \phi}{\partial y^2}\frac{\partial^2 w}{\partial x^2} - \frac{\partial^2 \phi}{\partial x^2}\frac{\partial^2 w}{\partial y^2} + 2\frac{\partial^2 w}{\partial x \partial y}\frac{\partial^2 \phi}{\partial x \partial y}$$

$$+P_{12}B_{11}\frac{\partial^4 \phi}{\partial y^4} + P_{12}B_{22}\frac{\partial^4 \phi}{\partial x^4} - (P_{11}B_{11} + P_{22}B_{22})\frac{\partial^4 \phi}{\partial x^2 \partial y^2} + C\dot{w} + \rho h \ddot{w} =$$

$$p(x,y,t) - k_z w(x_s, y_s, t),$$

(15)

where R_x and R_y are the radii of curvature in the x- and y-directions respectively, C is the viscous damping, h is the thickness, ρ the density of the plate, k_z is the stiffness of a support to which the plate may be attached, and $p(x,y,t)$ is the external excitation. For a detailed derivation see for example [33]. The coefficients P_{ij} are given by

$$(P_{11}, P_{12}, P_{22}) = \frac{(A_{22}, A_{12}, A_{11})}{A_{11}A_{22} - A_{12}^2},$$

(16)

$$P_{33} = \frac{1}{A_{66}}.$$

(17)

The compatibility equation is obtained from the elasticity relations for a body subject to a state of plane stress [26], and may be written as

$$P_{11}\frac{\partial^4 \phi}{\partial y^4} + P_{22}\frac{\partial^4 \phi}{\partial x^4} + (P_{33} - 2P_{12})\frac{\partial^4 \phi}{\partial x^2 \partial y^2} = P_{12}B_{11}\frac{\partial^4 w}{\partial x^4} + P_{12}B_{22}\frac{\partial^4 w}{\partial y^4}$$

$$-(P_{11}B_{11} + P_{22}B_{22})\frac{\partial^4 w}{\partial x^2 \partial y^2} + \frac{1}{R_x}\frac{\partial^2 w}{\partial y^2} + \frac{1}{R_y}\frac{\partial^2 w}{\partial x^2} + (\frac{\partial^2 w}{\partial x \partial y})^2 - \frac{\partial^2 w}{\partial x^2}\frac{\partial^2 w}{\partial y^2},$$

(18)

where Airy's stress function $\phi(x,y,t)$ is defined as

$$N_{xx} = \frac{\partial^2 \phi}{\partial y^2}, N_{yy} = \frac{\partial^2 \phi}{\partial x^2}, N_{xy} = -\frac{\partial^2 \phi}{\partial x \partial y},$$

(19)

15

(see for example [34]).

Equations (15) and (18) govern the dynamics of the transverse displacement of the bi-stable composite confined to one stable state, thus no changes between stable states or snap-through are accounted for. These equations are solved using a Galerkin approach, as outlined in [35]. Both the transverse displacement $w(x, y, t)$ and the stress function $\phi(x, y, t)$ are defined in the same domain and therefore it is assumed that they can be expanded in the same shape functions $w_{(i,j)}(x, y)$. This is exact, for the case of a simply supported plate with homogeneous material properties subject to small deflections [36]. For the case being considered here, this is an approximation due to the coupling between in-plane and transverse deflections caused by the curvature and unsymmetrical lamination. However, for shallow shells this approximation yields very good results [41]. Therefore, the solution for the transverse displacement and stress functions are written as

$$w(x, y, t) = \sum_{i=0}^{N} \sum_{j=0}^{N} w_{(i,j)}(x, y) W_{ij}(t), \tag{20}$$

$$\phi(x, y, t) = \sum_{m=0}^{N} \sum_{n=0}^{N} w_{(m,n)}(x, y) F_{ij}(t), \tag{21}$$

where $w_{ij}(x, y)$ are the shape functions given in Eq. (11), and, $W_{(i,j)}(t)$ and $F_{(m,n)}(t)$ are the displacement and stress function time response coefficients for shape function (i, j) and (m, n), the parenthesis in the equations for time responses $W_{(i,j)}(t)$ and $F_{(m,n)}(t)$ are dropped for clarity. Note that the first term in Eq. (20), $i, j = 0$, corresponds to a purely rigid body translation of the bi-stable plate in the out-of-plane direction, given by the term $\cos\left(\frac{\pi x 0}{L_x}\right) \cos\left(\frac{\pi y 0}{L_y}\right)$ in Eq. (11). In addition to this rigid body mode, rota-

16

tional rigid body modes with respect to the in-plane directions also result in out-of-plane displacements of the bi-stable plate. For the case where the studied composite is attached to an elastic support as the one described in Eq. (6), these rigid body modes will have a non-zero modal frequency. It is assumed that the torsional rigidity of the support is large, thus only the translational mode $(S, S)_0^w$ is considered in the derivation neglecting the rotational modes $(0, 0)_x$, $(0, 0)_y$ and $(0, 0)_z$.

In order to obtain a solution for the transverse displacement the expansions for the transverse displacement and the stress function, Eqs. (20) and (21), are substituted in the governing equations given by Eqs. (15) and (18)

to obtain

$$\sum_{i=0}^{N}\sum_{j=0}^{N}\left[(D_{11}-P_{11}B_{11}^2)w_{ij}^{''''}(x,y)+(D_{22}-P_{22}B_{22}^2)w_{ij}^{****}(x,y)\right]W_{ij}(t)$$

$$+\sum_{i=0}^{N}\sum_{j=0}^{N}2(D_{12}+P_{12}B_{11}B_{22}+2D_{33})w_{ij}^{''**}(x,y)W_{ij}(t)$$

$$+\sum_{m=0}^{N}\sum_{n=0}^{N}\left[\frac{1}{R_y}w_{mn}^{''}(x,y)+\frac{1}{R_x}w_{mn}^{**}(x,y)\right]F_{mn}(t)$$

$$+\sum_{m=0}^{N}\sum_{n=0}^{N}\left[P_{12}B_{11}w_{mn}^{''''}(x,y)+P_{12}B_{22}w_{mn}^{****}(x,y)\right]F_{mn}(t)$$

$$-\sum_{m=0}^{N}\sum_{n=0}^{N}(P_{11}B_{11}+P_{22}B_{22})w_{mn}^{''**}(x,y)F_{mn}(t)-$$

$$\sum_{i=0}^{N}\sum_{j=0}^{N}\sum_{m=0}^{N}\sum_{n=0}^{N}\left[(w_{ij}^{''}(x,y)w_{mn}^{**}(x,y)+w_{ij}^{**}(x,y)w_{mn}^{''}(x,y)\right]W_{ij}(t)F_{mn}(t)$$

$$+\sum_{i=0}^{N}\sum_{j=0}^{N}\sum_{m=0}^{N}\sum_{n=0}^{N}\left[2w_{ij}^{'*}(x,y)w_{mn}^{'*}(x,y)\right]W_{ij}(t)F_{mn}(t)$$

$$+\sum_{i=0}^{N}\sum_{j=0}^{N}w_{ij}(x,y)C_{ij}\dot{W}_{ij}+\sum_{i=0}^{N}\sum_{j=0}^{N}w_{ij}(x,y)\rho h\ddot{W}_{ij}=p(x,y,t)-\sum_{i=0}^{N}\sum_{j=0}^{N}k_z w_{ij}(x,y)W_{ij}$$

$$(22)$$

18

and

$$\sum_{m=0}^{N}\sum_{n=0}^{N}\left[P_{22}w_{mn}''''(x,y) + P_{11}w_{mn}^{****}(x,y) + (P_{33} - 2P_{12})w_{mn}''^{**}(x,y)\right]F_{mn}(t)$$

$$= \sum_{i=0}^{N}\sum_{j=0}^{N}\left[\frac{1}{R_y}w_{ij}''(x,y) + \frac{1}{R_x}w_{ij}^{**}(x,y)\right]W_{ij}(t)$$

$$+ \sum_{i=0}^{N}\sum_{j=0}^{N}\left[P_{12}B_{11}w_{ij}''''(x,y) + P_{12}B_{22}w_{ij}^{****}(x,y)\right]W_{ij}(t)$$

$$- \sum_{i=0}^{N}\sum_{j=0}^{N}\left[(P_{11}B_{11} + P_{22}B_{22})w_{ij}''^{**}(x,y)\right]W_{ij}(t)$$

$$+ \sum_{i=0}^{N}\sum_{j=0}^{N}\sum_{p=0}^{N}\sum_{q=0}^{N}\left[w_{ij}'^{*}(x,y)w_{pq}'^{*}(y) - w_{ij}''(x,y)w_{pq}^{**}(x,y)\right]W_{ij}(t)W_{pq}(t),$$

(23)

where $\{\}^{*}$ and $\{\}'$ indicate differentiation with respect to x and y respectively and the summation indices m, n have been used for ϕ, and, i, j and p, q for the cases where w is multiplied by another w term. Following the Galerkin procedure a set of modal nonlinear equations is obtained by projecting the solution onto shape functions given in Eq. (11), leading to a system of two coupled nonlinear equations of dimension $2(N \times N)$ each. This is achieved by multiplying Eq. (22) by arbitrary shape functions $w_{(a,b)}$, and Eq. (23) by arbitrary shape functions $w_{(m,n)}$, integrating over the surface of the shell and using the orthogonality conditions of the shape functions, given in Appendix B, to obtain

$$\ddot{W}_{ab} + 2\zeta_{ab,plate}\omega_{ab,plate}\dot{W}_{ab} + \omega_{ab,plate}^2 W_{ab} + ([\Gamma_{ab}] + [\Xi_{ab}])F_{ab}$$

$$+ \sum_{k=0}^{N}\sum_{l=0}^{N}\sum_{p=0}^{N}\sum_{q=0}^{N}\left[\Pi_{ab}^{klpq}\right]W_{kl}F_{pq} = \mathcal{Q}_{ab} - \mathcal{K}_{ab}^z W_{ab}$$

(24)

and

$$F_{mn} = [G_{mn}]^{-1} \left([H_{mn}] + [N_{mn}]\right) W_{mn} + \sum_{i=0}^{N} \sum_{j=0}^{N} \sum_{p=0}^{N} \sum_{q=0}^{N} [G_{mn}]^{-1} \left[T_{mn}^{ijpq}\right] W_{ij} W_{pq},$$

(25)

where $[G]$, $[H]$, $[N]$, $[T]$, $[\Gamma]$, $[\Pi]$ and $[\Xi]$ are coefficients depending on the mode shapes, $\mathcal{Q}_{ab}$ is the modal participation factor for mode (a, b) due to the external forcing, $\mathcal{K}_{ab}^{z}$ is the stiffness term due to the elastic support in the z-direction, and, $\omega_{ab,plate}$ and $\zeta_{ab,plate}$ are the natural frequency and damping ratio without including the curvature effect for mode (a, b). The definition of the coefficients multiplying the time response functions for the deflection W and stress function F in Eqs. (22) and (23) are given in Appendix B. Notice that since the shape functions for both the transverse displacement and the stress functions are sinusoidal functions, the stress function time response is decoupled from the transverse displacement in Eq. (25). This allows us to decouple the system of equations and write the governing equation of motion for the transverse displacement by substituting the expressions for $F_{(m,n)}$ in Eq. (24) as

$$\ddot{W}_{ab} + 2\zeta_{ab}\omega_{ab}\dot{W}_{ab} + \omega_{ab}^{2}W_{ab}$$
$$+ \sum_{i=0}^{N} \sum_{j=0}^{N} \sum_{p=0}^{N} \sum_{q=0}^{N} \left([G_{ab}]^{-1} \left([\Gamma_{ab}] + [\Xi_{ab}]\right) \left[T_{ab}^{ijpq}\right]\right) W_{ij} W_{pq}$$
$$+ \sum_{i=0}^{N} \sum_{j=0}^{N} \sum_{m=0}^{N} \sum_{n=0}^{N} \left([[G_{ab}]^{-1} \left([H_{ab}] + [N_{ab}]\right) \Pi_{ab}^{ijpq}]\right) W_{ij} W_{ab}$$
$$+ \sum_{i=0}^{N} \sum_{j=0}^{N} \sum_{p=0}^{N} \sum_{q=0}^{N} \sum_{m=0}^{N} \sum_{n=0}^{N} [G_{ab}]^{-1} \left[T_{ab}^{ijpq}\right] \left[\Pi_{ab}^{ijmn}\right] W_{ij} W_{pq} W_{ab} = \mathcal{Q}_{ab} - \mathcal{K}_{ab}^{z} W_{ab},$$

(26)

where ω_{ab} and ζ_{ab} are the natural frequency and damping ratio including the curvature effects, accounted by term $[G_{ab}]^{-1}\left([\Gamma_{ab}]+[\Xi_{ab}]\right)\left([H_{ab}]+[N_{ab}]\right)$, for mode (a,b). Equation (26) gives the modal equation for the time response W_{ab} of mode (a,b), including all possible modal interactions. The solution for the time response coefficients along with the corresponding mode shapes, are substituted in Eq. (20) to obtain the solution for the transverse nonlinear vibration of a bi-stable composite.

3. Dynamic response

The dynamics of a test specimen are experimentally studied to identify the existence of important nonlinear phenomena in the response of the bi-stable plate following the procedure detailed in Ref. [17]. These results allow for identifying nonlinear oscillations of the tested plate as well as to validate the derived model, as detailed in section 5. A bi-stable composite plate with unsymmetric stacking sequence $[0_4 - 90_4]_T$ and dimension 300 by 300 mm is used as the specimen for this study. The radii of curvature of the specimen R_x and R_y are 0.9 m and 10 m, respectively. The material properties of the specimen are given in Table 2. A schematic diagram of the plate in the stable configuration studied throughout this paper is shown in Fig. 3. In this state, the x-direction and y-direction are aligned with the larger and smaller curvatures of the plate, i.e. with the directions of principal curvature. The measured points P_x and P_y lie just off lines crossing at centre of the plate parallel to the x- and y-directions, as shown in Fig. 3. The experimental assembly showing both stable states of the bi-stable plate are shown in Fig. 4. The plate is mounted to an electromechanical shaker from its centre point and

Property	Value
$Fibrevol.\ [\%]$	57.7
$Ply\ thickness\ [mm]$	0.131
$Density\ \rho\ [kg/m^3]$	1570
$E_{xx}\ [GPa]$	164
$E_{yy}\ [GPa]$	12
$G^a_{xy}\ [GPa]$	4.6
$\nu^a_{xy} = \nu^a_{yx}$	0.3

Table 2: Material properties for a ply of HexPly 8557 IM7 used to manufacture the bi-stable plate experimental specimen.

the edges are unrestrained, resulting in a plate with free boundary conditions attached to an elastic support.
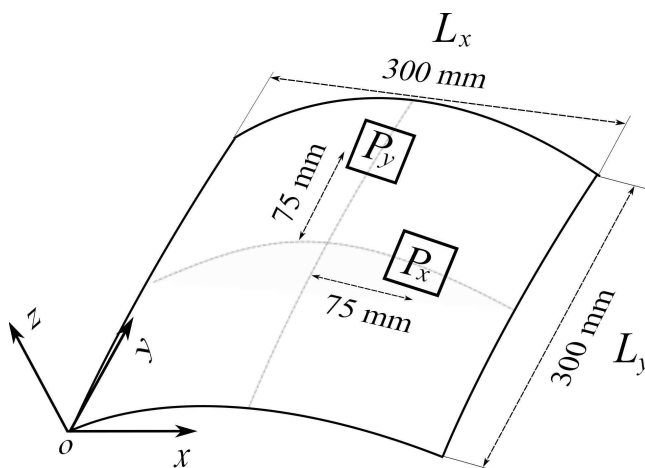

Figure 3: Measured points to study the out-of-plane displacement of the bi-stable plate.

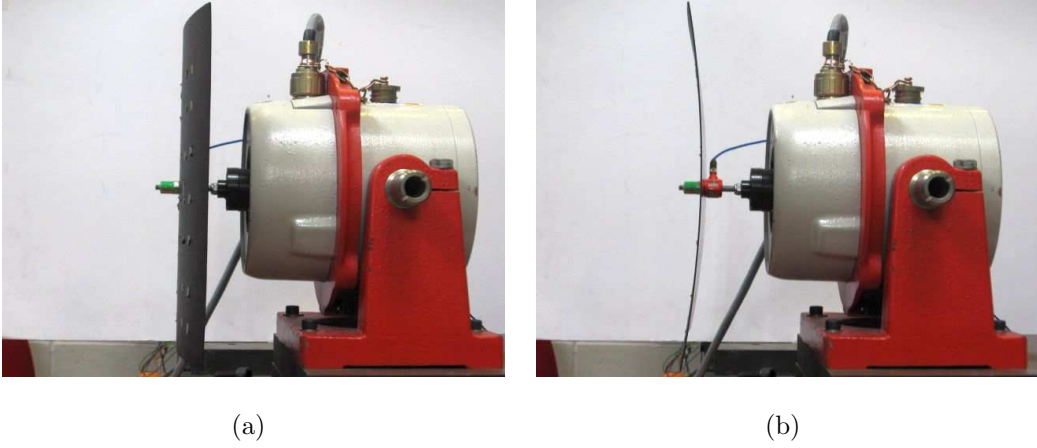Frequency response functions (FRF) [38] are obtained to study the low

Figure 4: Bi-stable plate mounted on Ling shaker, which is used as external excitation source. (a) Stable state 1. (b) Stable state 2. (Reproduced with the kind permission of the Journal of Intelligent Material Systems and Structures [39])

amplitude response of the specimen in the frequency range of interest for this work. This is chosen so it contains the frequencies for which snap-through is achieved with less actuation effort [39]. The FRF for point P_x for a low forcing amplitude of 1 N shows a linear response for this low level of excitation in Fig. 5. Three modes dominate the response of the specimen in this frequency range: mode w_1 at 17.6 Hz, mode w_2 at 19.4 Hz and mode w_3 at 45.4 Hz. Comparing the obtained theoretical modal frequencies with the experimental results it is observed that mode w_2 and w_3 correspond to theoretical modes $(A, A)_1^w$ and $(S, S)_1^w$, respectively. A distinct notation between theoretical modes (e.g. $(S, S)_0^w$) and experimental modes (e.g. w_1), will be used throughout the paper for differentiation. Mode w_1 does not relate to theoretical flexible modes, however inspecting its deflection shape, shown in Fig. 9(a), it corresponds to the rigid body translational mode in the out-of plate direction $(S, S)_0^w$, given in Fig. 2(f). In this case the modal

frequency is not zero as the plate is attached to an elastic support. This effect is taken into account by introducing a non-zero stiffness in the out-of-plane direction, k_z, in Eq. (6), the remaining elastic constants k_x and k_y are zero.
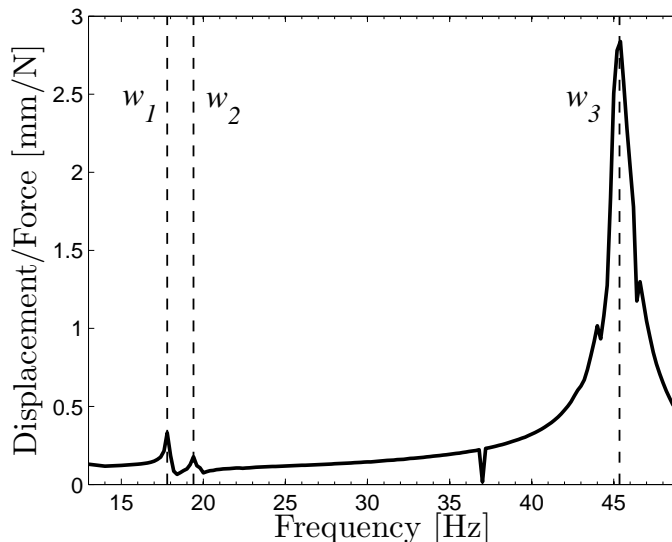

Figure 5: Experimental receptance (Displacement/Force) FRF for point P_x. Forcing amplitude $F_o = 1.0\ N$, frequency range $\Omega=[13, 49]$

In order to identify nonlinear oscillations, the forcing amplitude is increased and experimental frequency response diagrams are obtained using a stroboscopic sampling procedure detailed in Ref. [17]. These diagrams are obtained with single harmonic constant force stepped input sweeps. Peak-to-peak amplitudes of response are sampled over several consecutive forcing periods of steady state motions and plotted using the forcing frequency as parameter. For a linear response, a single amplitude value is sampled for consecutive periods for a given forcing frequency. Conversely, several points for a given frequency indicate the presence of multiple harmonics in the response

24

signalling nonlinear oscillations. The experimental frequency response diagram measured at point P_x for an input force amplitude of 5 N is shown in Fig. 6. The response is qualitatively similar to that observed in the linear FRF in Fig. 5, except for the regions around 35 Hz and 39 Hz. The multiple points shown in the experimental frequency response diagram in Fig. 6 indicate the appearance of nonlinear oscillations for these frequency ranges. Inspecting the time series for the deflection of point P_x presented in Fig. 7(a) for a forcing frequency of 34.4 Hz, we observe a non-sinusoidal response to a harmonic excitation of the plate. The power spectrum of this time response is presented in Fig. 7(b). It shows that most of the energy transmitted by the external forcing at 34.4 Hz, is transferred to a lower frequency at around 17.6 Hz. This frequency is very close to the experimentally identified modal frequency for mode w_1. The experimental observations for this nonlinear response show that as the forcing frequency is increased, the expected linear type response at the forcing frequency loses its stability. A completely different solution showing harmonics at the modal frequency and at twice the modal frequency (coinciding with the forcing frequency) appear around these frequency ranges. These characteristics match those of 1/2 subharmonic oscillations of mode w_1 [17, 40].

A similar behaviour can be seen for the experimental frequency response diagram measured at point P_y for the response of mode w_2, shown in Fig. 8. A dominant nonlinear response is seen around 39 Hz, this is at twice the modal frequency of mode w_2. This response was previously observed in Fig. 6, however its dominance is revealed in Fig. 8, showing an amplitude of response three times larger than the linear modal response of mode w_2. Once more,
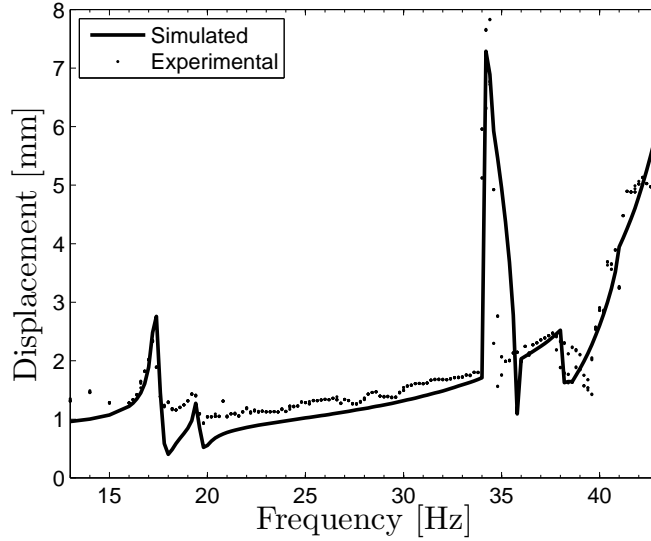
Figure 6: Experimental frequency response diagram for point P_x. F_o=5.0 N, frequency range Ω=[13, 43]

the experimental results agree with the characteristics of a $1/2$ subharmonic response of mode w_2. Although other sub- and super- harmonics were experimentally searched for, both at lower and higher frequencies, no others could be found for the chosen levels of forcing and the current plate configuration.

4. Low order model formulation

The main focus of this work is to develop a low order model for the transverse nonlinear dynamics of bi-stable composites confined to a stable state. Inspecting results from the associated linear eigenvalue problem, Eq. (13), it is noticed that very few shape functions are required to almost completely span the subspace of the first few transverse displacement eigenvectors. In particular, for the transverse displacement modes $(A, A)_1^w$, and $(S, S)_1^w$ vir-
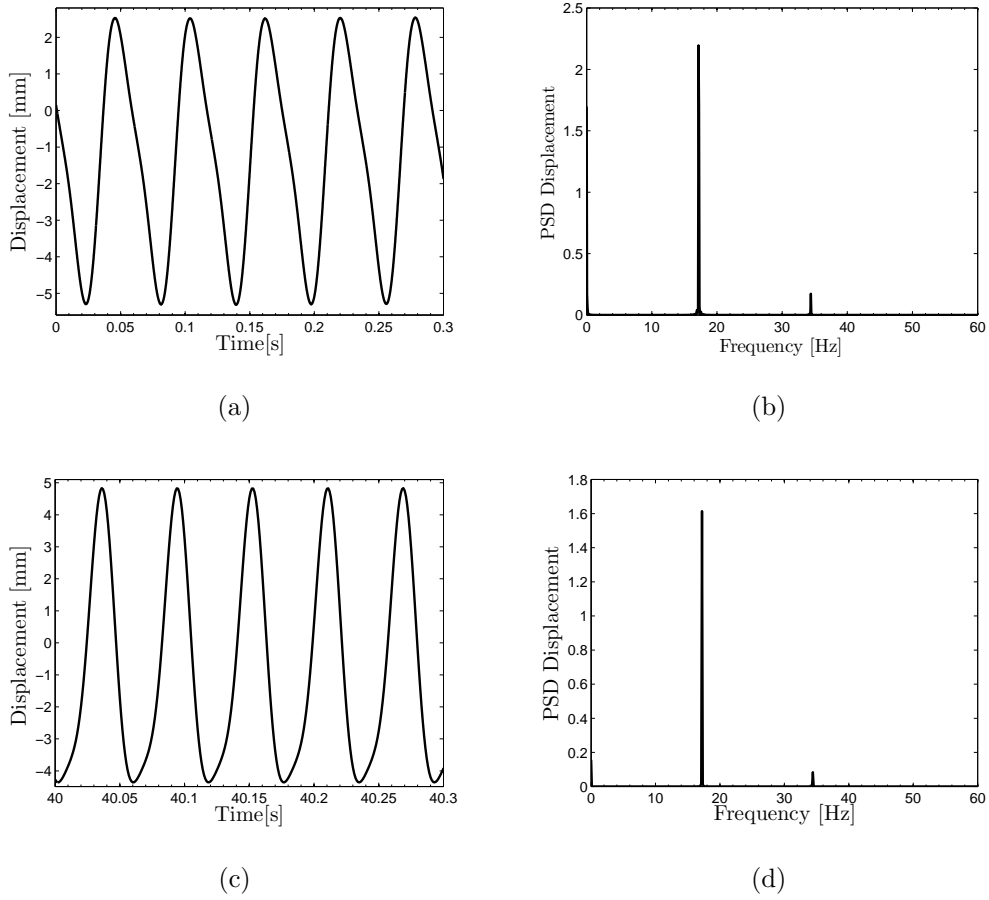
26

(a)

(b)

(c)

(d)

Figure 7: Experimental and simulated dynamic response for point P_x. Forcing amplitude F_o=5 N, forcing frequency Ω=34.4 Hz. (a) Experimental displacement time response. (b) Experimental displacement power spectrum. (c) Simulated displacement time response. (d) Simulated displacement power spectrum.

tually no coupling exists between in-plane and transverse terms. Furthermore, for these modes it is possible to closely approximate each mode shapes with only one shape function. Therefore, it is possible to treat these shape functions as eigenvectors of transverse displacement for modes $(A, A)_1^w$, and $(S, S)_1^w$. Furthermore, the rigid body translational mode $(S, S)_0^w$, shown in
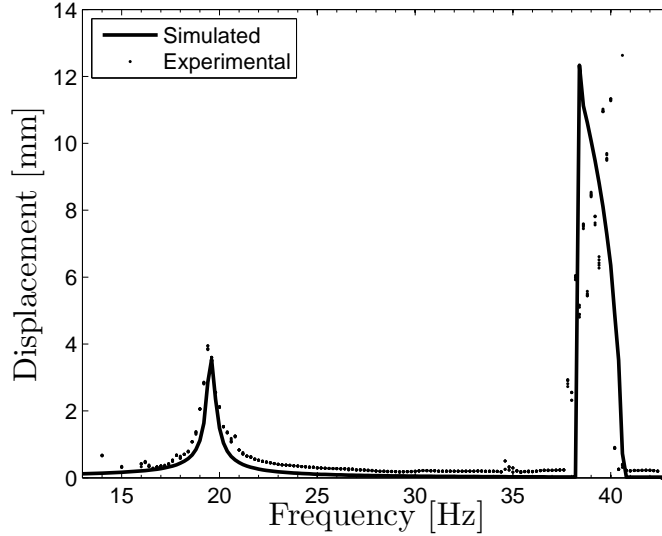
27

Figure 8: Experimental frequency response diagram for point P_y. Measured using strobo-scopic sampling for a forcing amplitude of $F_o = 5.0$ N, frequency range $\Omega=[13, 43]$

Fig. 2(f), is also closely approximated by a constant given by cosines terms in Eq. (11) and the shape function $w_{(S,S)_1}$. These theoretical results allow for truncating the number of terms used in the nonlinear problem solution, keeping only the relevant terms giving the eigenvectors of modes $(S, S)_0^w$, $(A, A)_1^w$, and $(S, S)_1^w$, i.e shape functions $w_{(S,S)_0}$, $w_{(A,A)_1}$, and $w_{(S,S)_1}$. Moreover, the previous discussion leading to an order reduction of the derived nonlinear model corresponds closely to the results from the dynamic characterisation presented in section 3. Thus, the solution for the transverse displacement w given by Eq. (20) can be truncated keeping only the first three shape functions in the expansion, i.e. $w_{(0,0)}$, $w_{(1,1)}$ and $w_{(1,0)}$ corresponding to theo-retical modes shapes $w_{(S,S)_0}$, $w_{(A,A)_1}$, and $w_{(S,S)_1}$ respectively. The truncated

28

solution for the transverse displacement is thus written as

$$w(x, y, t) = \sum_{i=0}^{N} \sum_{j=0}^{N} \left((w_{(0,0)} + w_{(1,0)}) W_{00}(t) + w_{(1,1)} W_{11}(t) + w_{(1,0)} W_{10}(t) \right) w_{ij}(x, y) W_{ij}(t),$$

(27)

where $W_{(0,0)}(t)$, $W_{(1,1)}(t)$ and $W_{(1,0)}(t)$, and, $w_{(0,0)}(x, y)$, $w_{(1,1)}(x, y)$, and $w_{(1,0)}(x, y)$ are the time response coefficients and mode shapes for theoretical modes $(S, S)_0^w$, $(A, A)_1^w$, and $(S, S)_1^w$ respectively. Following the Galerkin procedure by substituting Eq. (27) into Eq. (26), integrating over the shell domain, and dropping vanishing coefficients, the following nonlinear ordinary differential equations are obtained

$$\ddot{W}_{00} + 2\zeta_{00_w}\omega_{00_w}\dot{W}_{00} + \omega_{00_w}^2 W_{00} + \Phi_{1110}^{00_w}W_{11}W_{10} + \Phi_{0000}^{00}W_{00}W_{00} +$$

$$\Phi_{1100}^{00}W_{11}W_{00} + \Phi_{0010}^{00}W_{00}W_{10} + \Phi_{1111}^{00}W_{11}W_{11} + \Phi_{100110}^{00}W_{10}W_{01}W_{10} +$$

$$\Phi_{110110}^{00}W_{11}W_{01}W_{10} + \Phi_{110110}^{00}W_{11}W_{01}W_{10} + \Phi_{111110}^{00}W_{11}W_{11}W_{10} = \mathcal{Q}_{00}\sin(\Omega t),$$

(28)

$$\ddot{W}_{11} + 2\zeta_{w_{11}}\omega_{w_{11}}\dot{W}_{11} + \omega_{w_{11}}^2 W_{11} + \Phi_{1001}^{11}W_{10}W_{01} + \Phi_{1011}^{01}W_{10}W_{11} +$$

$$\Phi_{1101}^{11}W_{11}W_{01} + \Phi_{1111}^{11}W_{11}W_{11} + \Phi_{100111}^{11}W_{10}W_{01}W_{11} + \Phi_{110111}^{11}W_{11}W_{01}W_{11} +$$

$$\Phi_{101111}^{10}W_{10}W_{11}W_{11} + \Phi_{111111}^{11}W_{11}W_{11}W_{11} = \mathcal{Q}_{11}\sin(\Omega t),$$

(29)

$$\ddot{W}_{10} + 2\zeta_{w_{10}}\omega_{w_{10}}\dot{W}_{10} + \omega_{w_{10}}^2 W_{10} + \Phi_{1110}^{10}W_{11}W_{10} + \Phi_{1001}^{10}W_{10}W_{01} +$$

$$\Phi_{1101}^{10}W_{11}W_{01} + \Phi_{1010}^{10}W_{10}W_{10} + \Phi_{1111}^{10}W_{11}W_{11} + \Phi_{100110}^{10}W_{10}W_{01}W_{10} +$$

$$\Phi_{110110}^{10}W_{11}W_{01}W_{10} + \Phi_{110110}^{10}W_{11}W_{01}W_{10} + \Phi_{111110}^{10}W_{11}W_{11}W_{10} = \mathcal{Q}_{10}\sin(\Omega t),$$

(30)

where the coefficients Φ are calculated using Eq. (26) and the relations given in Appendix B, and $\omega_{w_{00}}$, $\omega_{w_{11}}$ and $\omega_{w_{10}}$ are the theoretical modal frequencies of modes $(S, S)_0^w$, $(A, A)_1^w$, and $(S, S)_1^w$ respectively.

To reduce the nonlinear terms in Eqs. (28)-(30), the experimental observations for the response of the plate are employed. First, only interactions between experimental modes w_1 and w_3, and modes w_2 and w_3, which correspond to theoretical modes $(S, S)_0^w$ and $(A, A)_1^w$, with mode $(S, S)_1^w$ are experimentally observed. Thus, all terms leading to other modal interactions are dropped. Second, only 1/2 subharmonic oscillations of modes w_1 and w_2 were observed in the response. Therefore, quadratic terms alone are kept in the equations to account for this dominant nonlinear response [42, 43, 44], allowing us to neglect cubic terms which lead to 1/3 sub- and super-harmonic oscillations not observed for the current configuration. This last simplification agrees with previous theoretical and experimental studies of shells, where cubic terms have been neglected as the quadratic terms arising from the curvature dominate the response of such structures [22]. Finally, the values of the nonlinear coefficients remaining in the governing equations are identified from the experimental frequency response diagrams.

Now we can rewrite equation Eqs. (28)-(30) for a sinusoidal forcing in the centre of the plate to obtain the reduced set nonlinear modal equations as

$$\ddot{W}_{00} + 2\zeta_{w_1}\omega_{w_1}\dot{W}_{00} + \omega_{w_1}^2 W_{00} + \alpha_{11}W_{00}^2 + \alpha_{13}W_{00}W_{10} = \mathcal{Q}_{00}\sin(\Omega t), \quad (31)$$

$$\ddot{W}_{11} + 2\zeta_{w_2}\omega_{w_2}\dot{W}_{11} + \omega_{w_2}^2 W_{11} + \alpha_{22}W_{11}^2 + \alpha_{23}W_{11}W_{10} = \mathcal{Q}_{11}\sin(\Omega t), \quad (32)$$

$$\ddot{W}_{10} + 2\zeta_{w_3}\omega_{w_3}\dot{W}_{10} + \omega_{w_3}^2 W_{10} = \mathcal{Q}_{10}\sin(\Omega t), \quad (33)$$

where $W_{(0,0)}(t)$ is the time response coefficient of the transverse displacement

30

for mode w_1 with natural frequency $\omega_{w_1} = 17.6$ Hz, $W_{(1,1)}(t)$ is the time response coefficient of the transverse displacement for mode w_2 with natural frequency $\omega_{w_2} = 19.4$ Hz, $W_{(1,0)}(t)$ is the time response coefficient of the transverse displacement for mode w_3 with natural frequency $\omega_{w_3} = 45.4$ Hz, Ω is the forcing frequency, $\mathcal{Q}_{ij}$ is the modal participation factor for mode w_i given in Appendix B, α_{ij} is the coefficient for the nonlinear quadratic term for an interaction between modes (w_i, w_j). The system of reduced Eqs. (31)-(33) gives the time response for the set of modes kept in the low order model. These equations are solved numerically to obtain simulated modal time functions for the transverse deflection. The complete solution is obtained by substituting the modal time functions along with the associated mode shapes obtained from Eq. (13), into Eq. (20).

5. Simulations and model validation

The reduced set of nonlinear equations for the modal time responses given by Eqs. (31)-(33) are solved using a Runge-Kutta type solver. The coefficients for the equations of motion are identified using experimental frequency response diagrams obtained as detailed in section 3. The parameters used in the simulations for equations Eqs. (31)-(33) are given in Table 3. The numerical solution for the reduced set of equations in the derived model is used to calculate the simulated dynamic response of the bi-stable plate and compared to the experimental results. The simulated frequency response diagram for point P_x is presented in Fig. 6 in a solid line and compared with the experimental results shown by dots. It can be seen that the simulated results are in good agreement with the experimental results. Furthermore,

Parameter	Value
ω_{w_1} [Hz]	17.6
ω_{w_2} [Hz]	19.4
ω_{w_3} [Hz]	45.4
ζ_{w_1}	0.01
ζ_{w_2}	0.01
ζ_{w_3}	0.03
α_{11}	300000
α_{13}	680000
α_{22}	680000
α_{23}	700000
$\mathcal{Q}_{10}$	0.088
$\mathcal{Q}_{01}$	0.0035
$\mathcal{Q}_{11}$	1.02

Table 3: Parameters used in numerical simulations.

comparing the displacement and power spectrum graphs of point P_x for a forcing frequency Ω of 34.4 Hz, given in Figs. 7(c)-7(d), with the experimental results, shown in Figs. 7(a)-7(b), the ability of the model to capture even detailed dynamic features is highlighted. In addition, a comparison between the experimental and simulated frequency response diagrams for point P_y is shown in Fig. 8. As for point P_x, a close quantitative and qualitative match is achieved.

6. Spatial response comparison

Experimental deflection shapes are obtained and compared to theoretical mode shapes. The experimental deflection shapes are obtained by exciting the plate with sinusoidal inputs for a forcing frequency equal to the frequency of the relevant modes. Additionally, deflection shapes for the ranges of subharmonic oscillations are also obtained. The measurements are performed for a range of forcing amplitudes between $[0.5, 5]$ N in both stable states for each of the dominant modes and subharmonic oscillations in order to detect possible amplitude dependent deflection shapes. The experimental results for both stable states are virtually identical, and for illustration we use those obtained for state one. A Polytec OFV056/3001 scanning laser vibrometer is used to acquire instant displacement for a grid of point on the bi-stable plate surface. The software provided by the laser vibrometer manufacturer is used to construct the deflection shapes. The algorithm obtains amplitude and phase information for each point on the grid. The displacement in space of these points is measured with respect to a plane (shown as a squared grid in Figs. 9(a), 9(b), 10(a), 10(b), 11(a), 11(b), 12 and 13), from which the deflected shapes can be inferred based on the assumption that the static curvature is small (see section 2 and Fig. 1).

Figures 9(a) and 9(b) show the experimental and simulated mode shapes for mode w_1. Comparing the measured deflection shape shown in Figs. 9(a) and 9(b) with the simulated mode shape in Figs. 9(c) and 9(d), a good qualitative match is achieved using the mode shapes from the linear associated problem. As in Fig. 2, the simulated mode shapes (deformed shapes) in Figs. 9(c), 9(d), 10(c), 10(d), 11(c) and 11(d) are shown with respect to
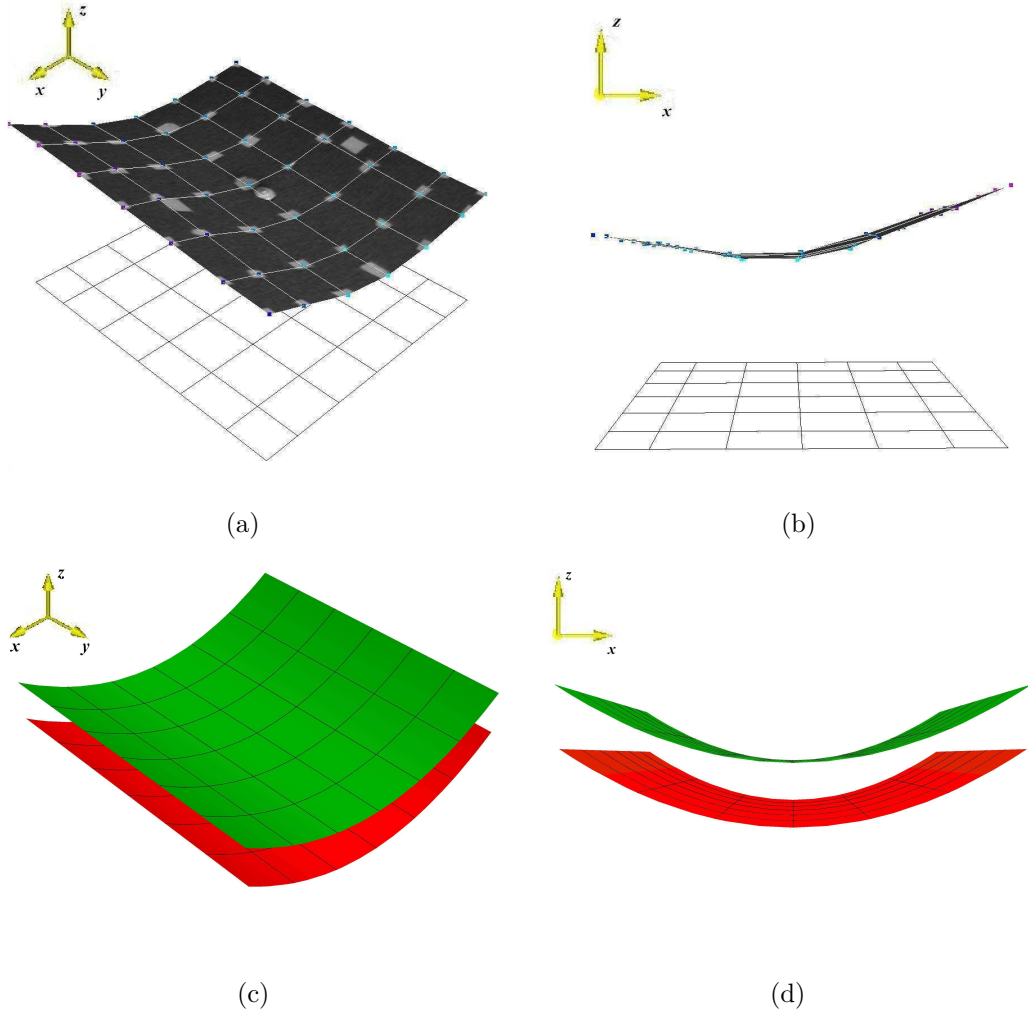
33

(a)   (b)

(c)   (d)

Figure 9: Comparison between experimental deflections shapes for mode w_1 and mode shapes obtained from Eq. (13) for mode $(S, S)_0^w$. (a) 3-D view of the experimental deflection shape for mode w_1. (b) Lateral view (ZX plane) of the experimental deflection shape for mode w_1. (c) 3-D view of simulated mode shape (deformed shapes) $w_{(S,S)_0}(x, y)$. (d) Lateral (ZX plane) view of simulated mode shape (deformed shapes) $w_{(S,S)_0}(x, y)$.

the undeformed shape of the bi-stable plate plotted in green. Experimental deflection shapes for higher levels of forcing for the dominant modes are ob-

34

tained, however no amplitude dependent behaviour is observed, hence these images are omitted. The mode shapes and the experimental deflection shapes for modes w_2 and w_3 are also compared in Figs. 10 and 11, respectively. For mode w_2 the experimental deflection shape differs from the calculated mode shape. The observed mismatch may be explained by the effects added by the non perfect support and small geometrical imperfections in the shape of shells, as a non-uniform curvature, which can largely alter the actual shape of the deflection [22, 31]. For mode w_3 very good agreement between the measured deflection shape and calculated mode shape is achieved as seen in Fig. 11. This is a very relevant result since this mode dominates the dynamic behaviour in the frequency range of interest, which potentially allows us to use the model for morphing shape and vibration suppression control of bi-stable composites.

The deflection shapes for the subharmonic oscillations are also studied. Figure 12 shows the deflection shape for a forcing amplitude of 1 N and a forcing frequency of 34.8 Hz. For this level of forcing no subharmonic response is observed (see Fig. 12), thus the measured shape matches that observed for mode w_3 as it dominates the linear response in this range of frequencies. As the forcing amplitude is increased and the subharmonic instability is triggered, the plate response shows two dominant harmonics, at the forcing frequency and at half the forcing frequency. The corresponding deflection shapes are shown in Figs. 13(a) and 13(b). In view of this, the actual deflection shape for the subharmonic response is assumed to be the sum of the linear response dominated by mode w_3, and the response due to the subharmonic resonance of mode w_1. Inspecting Figs. 12 and 13(b),

<center>(a)</center>

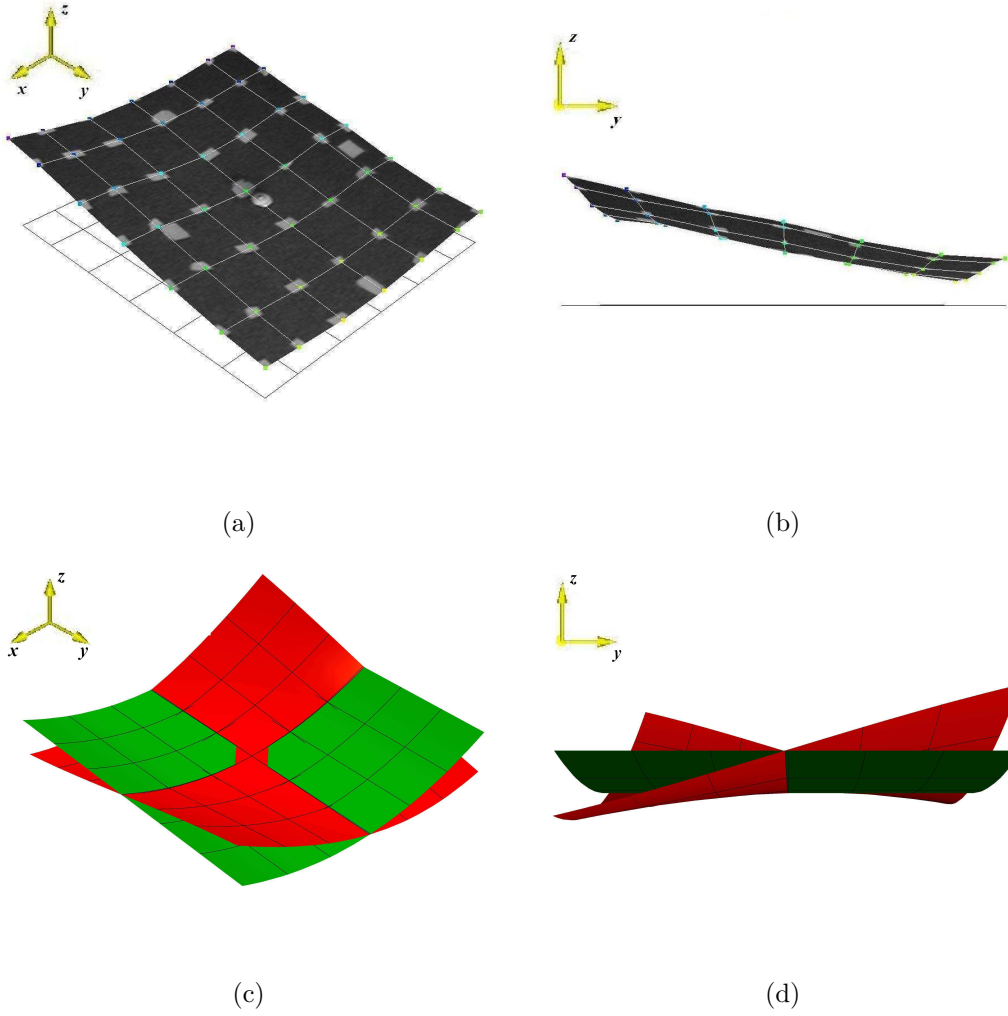<center>(b)</center>

<center>(c)</center>

<center>(d)</center>

Figure 10: Comparison between experimental deflections shapes for mode w_2 and mode shapes obtained from Eq. (13) for mode $(A, A)_1^w$. (a) 3-D view of the experimental deflection shape for mode w_2. (b) Lateral view (ZY plane) of the experimental deflection shape for mode w_2. (c) 3-D view of simulated mode shape $w_{(A,A)_1}(x,y)$. (d) Lateral (ZY plane) view of simulated mode shape $w_{(A,A)_1}(x,y)$.

the deflection shape due to the response of the harmonic at the forcing frequency of the subharmonic oscillations shows the same shape as mode w_3.
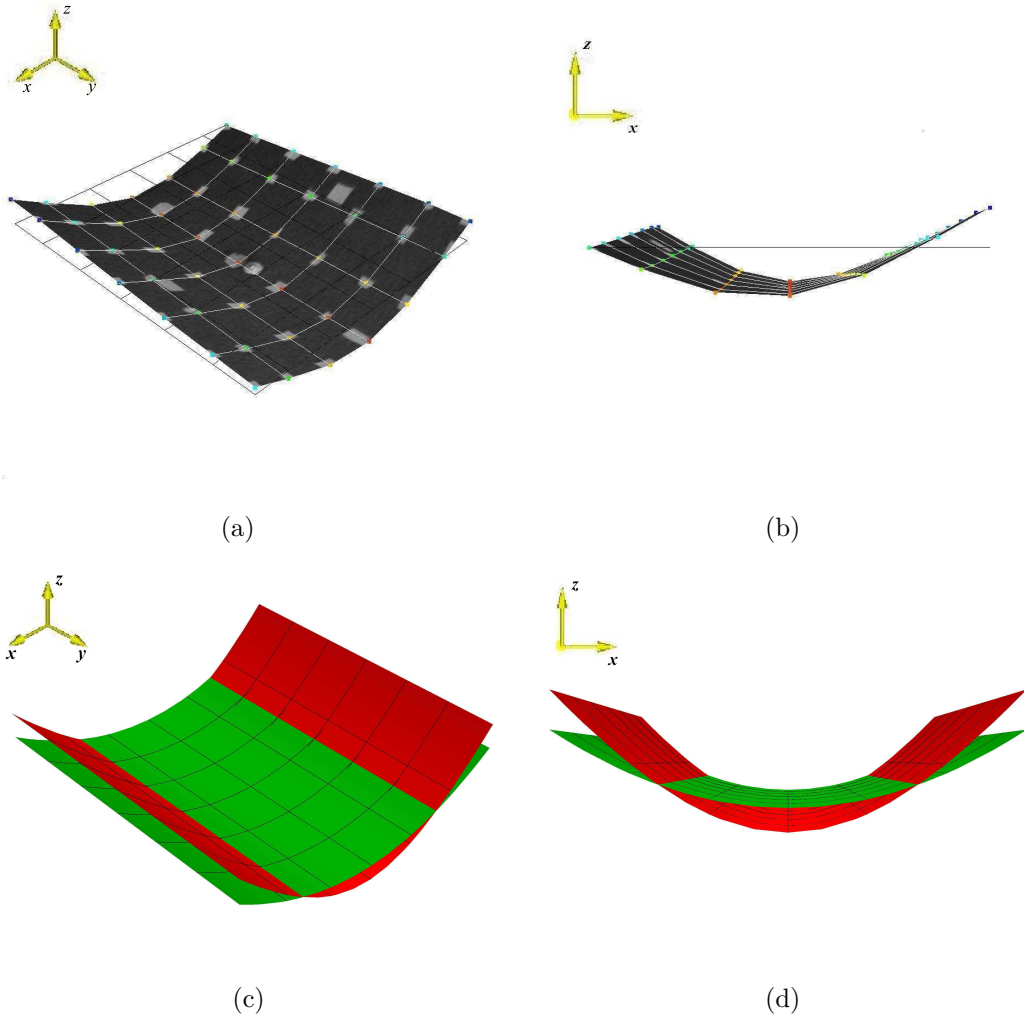
<center>36</center>

(a)

(b)

(c)

(d)

Figure 11: Comparison between experimental deflections shapes for mode w_3 and mode shapes obtained from Eq. (13) for mode $(S, S)_1^w$. (a) 3-D view of the experimental deflection shape for mode w_3. (b) Lateral view (ZX plane) of the experimental deflection shape for mode w_3. (c) 3-D view of simulated mode shape $w_{(S,S)_1}(x, y)$. (d) Lateral (ZX plane) view of simulated mode shape $w_{(S,S)_1}(x, y)$.

On the other hand, the deflection shape due to the response of the harmonic at half the forcing frequency, is slightly different showing no curvature with
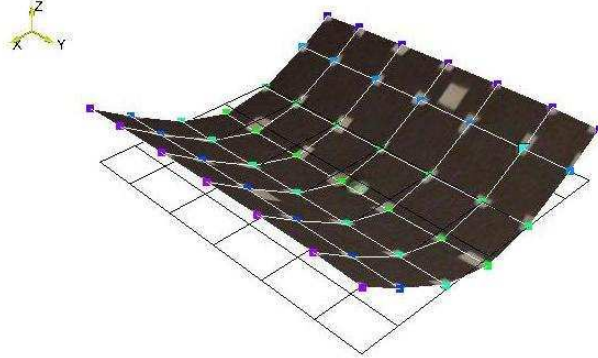
Figure 12: Experimental deflection shape for a forcing frequency of 34.8 Hz

respect to the x-direction deviating from the deflection shape of w_1, as can be seen by comparing Figs. 9(a) and 13(a). Hence, as the subharmonic oscillations are triggered, the deflection shape of the plate varies, resulting in an amplitude dependent behaviour of the spatial response. In spite of this, the measured nonlinear deflection shape behaviour is approximated by the model with the chosen mode shapes obtained from the associated linear problem, as explained in the following.

The time response of mode $W_{(0,0)}$ when the subharmonic oscillations are triggered is non-zero, this condition can be written as

$$
\begin{cases}
W_{(0,0)} = 0, & for \ F_0 < F_{sub_{w_1}} \\
\\
W_{(0,0)} \neq 0, & for \ F_0 \geq F_{sub_{w_1}}
\end{cases}
\tag{34}
$$

where F_0 is the forcing amplitude, and $F_{sub_{w_1}}$ is the forcing amplitude required to trigger the subharmonic oscillations for mode w_1 previously calculated in Ref. [17]. Thus, for $F_0 \geq F_{sub_{w_1}}$ the total response for the subhar-

monic oscillations associated to mode w_1 is given by

$$w_{1\,sub}(x, y, t) = (w_{(0,0)} + w_{(1,0)})W_{00}(t) + w_{(1,0)}W_{10}(t), \qquad (35)$$

as the response for $W_{(1,1)}$ is negligible for this frequency range. The total response for the subharmonic oscillations associated to mode w_2 can be obtained following a similar procedure using the results for $F_{sub_{w_2}}$ given in [17]. Equation (35) shows the ability of the derived model to qualitatively approximate the observed nonlinear deflection shape behaviour.
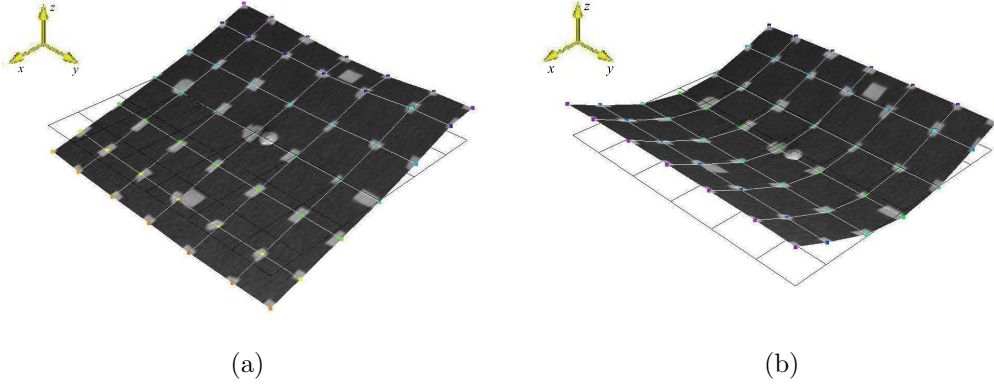

(a)   (b)

Figure 13: Experimental deflection shape for a subharmonic response. Forcing amplitude F_o=4 N, forcing frequency Ω=34.8 Hz. (a) Experimental deflection shape due to the response content at 17.6 Hz. forcing frequency of 34.8 Hz. (b) Experimental deflection shape due to the response content at 34.8 Hz.

7. Conclusions

A mathematical model to capture the dynamic response of bi-stable composite plates is derived using classical nonlinear shell theory. Modal equations for the time response and associated mode shapes are combined to obtain

the full response for the transverse displacement following a Rayleigh-Ritz-Galerkin approach. The number of modes in the general model is reduced based on theoretical results from the associated linear problem to obtain a low order model for the dynamics of bi-stable composites. The reduced model is validated comparing simulated results to the experimental response of a bi-stable plate test specimen. The experimentally observed subharmonic oscillations are modelled accurately with the nonlinearities kept in the low order model. In addition, the calculated modal frequencies from the associated linear problem are in good agreement with the experimental results providing an upper frequency bound for each mode.

Experimental deflection shapes are measured for the relevant modes of the plate and compared to theoretical mode shapes achieving good qualitative results. The deflection shapes for the subharmonic response ranges are also studied, revealing a quantitative change in deflection shape of the plate as these oscillations are triggered. The experimentally observed behaviour constitutes a rare bifurcation of the spatial response of a structure that deserves further investigation. This nonlinear behaviour in the shape of the deflection is approximately captured by the model. In addition, the frequency range of interest for morphing applications may be identified with the derived model by studying the symmetry of mode shapes with respect to the flat direction of bi-stable composites, since this yields the modes requiring less actuation effort to trigger snap-through. This is an important design feature to be exploited for developing efficient morphing strategies and stability control to prevent undesired snap-through for bi-stable composite applications.

Acknowledgements

A. Components of the mass and stiffness matrices

The mass matrix $\mathbf{M}$ in Eq. (13) is given by

$$
\begin{bmatrix}
M_{aijmn} & [0] & [0] \\
[0] & M_{bijmn} & [0] \\
[0] & [0] & M_{cijmn}
\end{bmatrix},
\tag{A.1}
$$

where the coefficients are

$$
M_{aijmn} = \rho h \int_0^{L_x} \int_0^{L_y} (u_{ij} u_{mn}) \, dy dx,
\tag{A.2}
$$

$$
M_{bijmn} = \rho h \int_0^{L_x} \int_0^{L_y} (v_{ij} v_{mn}) \, dy dx,
\tag{A.3}
$$

$$
M_{cijmn} = \rho h \int_0^{L_x} \int_0^{L_y} (w_{ij} w_{mn}) \, dy dx.
\tag{A.4}
$$

The stiffness matrix $\mathbf{K}$ in Eq. (13) is given by

$$
\begin{bmatrix}
K^u_{aijmn} & K^u_{bijmn} & K^u_{cijmn} \\
K^u_{bijmn} & K^v_{bijmn} & K^v_{cijmn} \\
K^u_{cijmn} & K^v_{cijmn} & K^w_{cijmn}
\end{bmatrix}
\tag{A.5}
$$

41

where the coefficients are written as

$$K_{aijmn}^{u} = \int_0^{L_x} \int_0^{L_y} \left(A_{11}(u_{ij}^* u_{mn}^*) + A_{33}(u_{ij}' u_{mn}') \right) dxdy, \tag{A.6}$$

$$K_{bijmn}^{u} = \int_0^{L_x} \int_0^{L_y} \left(A_{12}(u_{ij}^* v_{mn}^*) + A_{33}(u_{ij}' v_{mn}^*) \right) dxdy, \tag{A.7}$$

$$K_{cijmn}^{u} = \int_0^{L_x} \int_0^{L_y} \left(A_{11} \left(u_{ij}^* \frac{w_{mn}}{R_x} \right) + A_{12} \left(u_{ij}^* \frac{w_{mn}}{R_y} \right) - B_{11} \left(u_{ij}^* w_{mn}^{**} \right) \right) dxdy \tag{A.8}$$

$$K_{bijmn}^{v} = \int_0^{L_x} \int_0^{L_y} \left(A_{22}(v_{ij}' u_{mn}') + A_{33}(v_{ij}^* v_{mn}^*) \right) dxdy, \tag{A.9}$$

$$K_{cijmn}^{v} = \int_0^{L_x} \int_0^{L_y} \left(A_{22} \left(v_{ij}' \frac{w_{mn}}{R_y} \right) + A_{12} \left(v_{ij}' \frac{w_{mn}}{R_x} \right) - B_{22} \left(v_{ij}' w_{mn}'' \right) \right) dxdy \tag{A.10}$$

$$K_{cijmn}^{w} = \int_0^{L_x} \int_0^{L_y} (A_{11} \left(w_{ij} \frac{w_{mn}}{R_x} \right) + A_{22} \left(w_{ij} \frac{w_{mn}}{R_y} \right) + 2A_{12} \left(\frac{w_{ij} w_{mn}}{R_x R_y} \right)$$

$$-B_{11} \left(\frac{w_{ij} w_{mn}^{**}}{R_y} \right) - B_{22} \left(\frac{w_{ij} w_{mn}^{**}}{R_y} \right) + D_{11} \left(w_{ij}^{**} w_{mn}^{**} \right)$$

$$+D_{22} \left(w_{ij}'' w_{mn}'' \right) + 2D_{12} \left(w_{ij}^{**} w_{mn}'' \right) + 4D_{33} \left(w_{ij}^{*'} w_{mn}^{*'} \right) + k_z w_{ij} w_{mn}) dxdy. \tag{A.11}$$

B. Orthogonality conditions and coeffients

The orthogonality conditions for sinusoidal functions used in Eqs. (25)-(26) are given by

$$\int_0^{L} \sin(\alpha mx) \sin(\alpha nx) = \begin{cases} 0, & for\ m \neq n \\ \\ \frac{L}{2}, & for\ m = n \end{cases} \tag{B.1}$$

$$\int_0^{L} \cos(\alpha mx) \cos(\alpha nx) = \begin{cases} 0, & for\ m \neq n \\ \\ \frac{L}{2}, & for\ m = n \end{cases} \tag{B.2}$$

42

$$\int_0^L \sin(\alpha m x) \cos(\alpha n x) = 0. \tag{B.3}$$

The coefficients used in Eqs. (25)-(26) are given by

$$\mathcal{K}_{ab}^z \;\; = \;\; \frac{k_z}{\omega_{ab,plate}^2 \rho h}, \tag{B.4}$$

$$\omega_{ab,plate}^2 \;\; = \;\; \frac{1}{\rho h}\left(\lambda_{x_a}^4\left(D_{11} - P_{11}B_{11}^2\right) + \lambda_{y_b}^4\left(D_{22} - P_{22}B_{22}^2\right)\right)$$
$$+\frac{1}{\rho h}2\lambda_{x_a}^2\lambda_{x_b}^2(D_{12} + P_{12}B_{11}B_{22} + 2D_{33}), \tag{B.5}$$

$$\omega_{ab}^2 = \omega_{ab,plate}^2 + \mathcal{K}_{ab}^z + [G_{ab}]^{-1}\left([\Gamma_{ab}] + [\Xi_{ab}]\right)\left([H_{ab}] + [N_{ab}]\right) \tag{B.6}$$

$$\zeta_{ab,plate} \;\; = \;\; \frac{C_{ab}}{\omega_{ab,plate}^2 \rho h}, \tag{B.7}$$

$$\zeta_{ab} \;\; = \;\; \frac{C_{ab}}{\omega_{ab}^2 \rho h}, \tag{B.8}$$

$$\Gamma_{ab} \;\; = \;\; \frac{1}{\rho h}\left(\frac{1}{R_x}\gamma_{y_b}^2 + \frac{1}{R_y}\gamma_{x_a}^2\right), \tag{B.9}$$

$$\Xi_{ab} \;\; = \;\; \frac{1}{\rho h}\left(\gamma_{y_b}^4 P_{12}B_{11} + \gamma_{x_a}^4 P_{12}B_{22} + \gamma_{x_a}^2\gamma_{y_b}^2(P_{11}B_{11} + P_{22}B_{22})\right), \tag{B.10}$$

$$\Pi_{ab}^{ijmn} = \frac{1}{L_x L_y \rho h}\left(-\lambda_{x_a}^2\gamma_{y_n}^2 \Phi_{ab}^{ijmn} - \gamma_{x_a}^2\lambda_{y_n}^2 \Phi_{ab}^{ijmn} + 2\lambda_{x_i}\lambda_{y_j}\gamma_{x_m}\gamma_{y_n} \Phi_{ab}^{ijmn}\right), \tag{B.11}$$

$$G_{ab} = \frac{L_x L_y}{4}\left(\gamma_{x_a}^4 P_{11} + \gamma_{y_b}^4 P_{22} + \gamma_{x_a}^2\gamma_{y_b}^2(P_{33} - 2P_{12})\right), \tag{B.12}$$

$$H_{ab} = \frac{L_x L_y}{4}\left(\frac{1}{R_x}\lambda_{x_a}^2 + \frac{1}{R_y}\lambda_{y_a}^2\right), \tag{B.13}$$

43

$$N_{ab} = \frac{L_x L_y}{4} \left(\lambda_{x_a}^4 P_{12} B_{11} + \lambda_{y_b}^4 P_{12} B_{22} - \lambda_{x_1}^2 \lambda_{x_b}^2 \left(P_{11} B_{11} + P_{22} B_{22} \right) \right), \text{ (B.14)}$$

$$T_{ab}^{ijmn} = \left(\lambda_{x_i} \lambda_{y_j} \gamma_{x_m} \gamma_{y_n} \Phi_{ab}^{ijmn} + \lambda_{x_i}^2 \gamma_{y_n}^2 \Phi_{ab}^{ijmn} \right), \quad \text{(B.15)}$$

$$\mathcal{Q}_{ab} = \frac{4}{L_x L_y \rho h} \int_0^{L_x} \int_0^{L_y} p(x, y, t) X_a(x) Y_b(y) dy dx, \quad \text{(B.16)}$$

$$\lambda_{x_a} = \left(\frac{\pi x a}{L_x} \right), \quad \text{(B.17)}$$

$$\gamma_{x_a} = \left(\frac{\pi x a}{L_x} \right), \quad \text{(B.18)}$$

where the coefficients Φ is defined as

$$\Phi_{ab}^{ijmn} = \int_0^{L_x} \int_0^{L_y} w_{(a,b)}(x, y) w_{(i,j)}(x, y) w_{(m,n)}(x, y) dy dx, \quad \text{(B.19)}$$

References

[1] M.-L. Dano, M.W. Hyer, Thermally-induced deformation behavior of unsymmetric laminates. *International Journal of Solids and Structures*, 35, (1998) 2101-2120.

[2] M. Schlecht, K. Schulte, Advanced calculation of the room-temperature shapes of unsymmetric laminates, *Journal of Composite Materials*, 33. (1999) 1472-1490.

[3] S.V. Sokorin, A.V. Terentiev, On Modal Interaction, Stability and Nonlinear Dynamics of a Model Two D.O.F. Mechanical System Performing Snap-Through Motion, Nonlinear Dynamics, 16, (1998) 239-257.

[4] M.R. Schultz, M.R. Hyer, Snap-through of Unsymmetric Cross-ply Laminates using Piezoceramic Actuators, *Journal of intelligent material systems and structures*, 14, (2003) 795-814.

[5] K. Potter, P.M. Weaver, A concept for the generation of out-of-plane distortion from tailored FRP laminates, *Composites Part A*, 35, (2004) 1353-1361.

[6] C. G. Diaconu, P. M. Weaver, F. Mattioni, Concepts for morphing airfoil sections using bi-stable laminated composite structures, *Thin-Walled Structures*, 46, (2008) 689-701.

[7] F. Mattioni, P.M. Weaver, K. Potter, M.I. Friswell, The application of residual stress tailoring of snap-through composites for variable sweep wings, *Proceedings of the 47th AIAA/ASME/ASCE/AHS/ASC Structures, Structural Dynamics, and Materials Conference*, Rhode Island, May (2006).

[8] M.-L. Dano, M.W. Hyer, Snap-through of unsymmetric fiber-reinforced composite laminates. *International Journal of Solids and Structures*, 39, (2002) 175-198.

[9] W. Hufenbach, M. Gude, L. Kroll, Design of multistable composites for application in adaptive structures, *Composites Science and Technology*, 62,(2002) 2201-2207.

[10] P. Giddings, C.R. Bowen, R. Butler, H.A. Kim, Characterisation of actuation properties of piezoelectric bi-stable carbon-fibre laminates, Composites Part. A, 39,(2008) 697-703.

[11] F. Mattioni, P.M. Weaver, K. Potter, M.I. Friswell, Analysis of thermally induced multistable composites, *International Journal of Solids and Structures*, 45, (2008) 657-675.

[12] M.-L. Dano, M.W. Hyer, SMA-induced snap-through of unsymmetric fiber-reinforced composite laminates, *International Journal of Solids and Structures*, 40, (2003) 5949-5972 .

[13] K. Potter, P. Weaver, A.A. Seman, S. Shah, Phenomena in the bifurcation of unsymmetric composite plates. *Composites Part A*, 35,(2006) 100-106.

[14] M.R Schultz, M.W. Hyer, R.B. Williams, W.K. Wilkie, D.J. Inman, Snap-through of unsymmetric laminates using piezocomposite actuators, *Composite Science and Technology*, 66, (2006) 2442-2448.

[15] C. G. Diaconu, P. M Weaver, A. F. Arrieta, Dynamic analysis of bistable composite plates, *Journal of Sound and Vibration*, 22, (2009) 987-1004.

[16] A.F. Arrieta, F. Mattioni, S.A. Neild, P.M. Weaver, D.J. Wagg, K. Potter, Nonlinear dynamics of a bi-stable composite laminate plate with applications to adaptive structures, *Proceedings of the 2nd European Conference for Aero-Space Sciences(EUCASS2007)*, Brussels, July (2007)

[17] A. F. Arrieta, S.A. Neild, D.J. Wagg, Nonlinear dynamic response and modelling of a bi-stable composite plate for applications to adaptive structures, *Nonlinear Dynamics*, 58, (2009) 259-272.

[18] A.W. Leissa, Y. Narita, Vibrations of completely free shallow shells of rectangular planform, *Journal of Sound and Vibration*, 96, (1984) 207-218.

[19] K. M. Liew and K. Y. Lam, Effects of Arbitrarily Distributed Elastic Point Constraints on Vibrational Behaviour of Rectangular Plates, *Journal of Sound and Vibration*, 174, (1994) 23-36.

[20] S. Hurlebaus, L. Gaul, J. T.-S. Wang. An exact series solution for calculating the eigenfrequencies of orthotropic plates with completely free boundarys, *Journal of Sound and Vibration*, 244, (2001) 747-759.

[21] O. Thomas, C. Touze, A. Chaigne, Asymmetric non-linear forced vibrations of free-edge circular plates. part ii: experiments. *Journal of Sound and Vibration*, 265, (2003) 1075-1101.

[22] O. Thomas, C. Touze, E Luminais, Non-linear vibrations of free-edge thin spherical shells: Experiments on a 1:1:2 internal resonance, *Nonlinear Dynamics*, 49, (2007) 259-284.

[23] A.H. Nayfeh, D.T. Mook, *Nonlinear Oscillations*. Wiley, New York, (1979).

[24] S. Lefschetz, *Modern Mathematics for the Engineer*. Mcgraw-Hill, New York, (1956).

[25] T. Von Karman, The Engineer Grapples With Nonlinear Problems. *Bulletin of American Mathematical Society*, 46,(1940) 615-683.

[26] A.H. Nayfeh, P.F. Pai, *Linear and Nonlinear Structural Mechanics*. Wiley, New York, (2004).

[27] E. Ventsel, T. Krauthammer, *Thin Plates and Shells: Theory: Analysis, and Applications*. Marcel Dekker, Inc., New York, (2001).

[28] P. Hagedorn and A. DasGupta *Vibration and Waves in Continuous Mechanical Systems.* John Wiley & Sons, Chichester, (2007).

[29] A.H. Nayfeh, *Introduction to Composite Materials*, Technomic Publishing Company, Inc., Lancaster, (1980).

[30] L. Meirovitch *Methods of Analytical Dynamics.* McGraw-Hill, New York, (1970).

[31] M. Amabili, *Nonlinear Vibrations and Stability of Shells and Plates*, Cambridge University Press, (2008).

[32] V. Z. Vlasov, Basic differential equations in the general theory of elastic shells, *NACA TM 1241*, 1951.

[33] D.J. Wagg, S.A. Neild, *Nonlinear vibration with control: for flexible and adaptive structures*, Springer, (2009).

[34] W. Nowacki, *Dynamics of Elastic Systems*, Wiley, (1963).

[35] C.-Y. Chia, *Nonlinear Analysis of Plates*, McGraw-Hill, (1980).

[36] A.W. Leissa, *Vibration of Shells*, National Aeronautics and Space Administration, (1971).

[37] A.W. Leissa, Free vibration of rectangular-plates, *Journal of Sound and Vibration*, 31, (1973) 257-293.

[38] D.J. Ewins., *Modal Testing*, Research studies press LTD., Baldock, (2000).

[39] A. F. Arrieta, D.J. Wagg, S.A. Neild, Dynamic snap-through for morphing of bi-stable composite plates, *Journal of Intelligent Material Systems and Structures*, in Press, (2010).

[40] A.H. Nayfeh, *Nonlinear Interactions, Analytical, Computational, and Experimental Methods*, Wiley, New York, (2000).

[41] W. Soedel, *Vibration of shells and plates*, Marcel Dekker, Inc., (2004).

[42] B. Balachandran, A.H. Nayfeh, Observations of Modal Interactions in Resonantly Forced Beam-Mass Structures, *Nonlinear Dynamics*, 2, (1991) 77-117.

[43] S.H. Chen, Y.K. Cheung, H.X. Xing, Nonlinear Vibration of Plane Structures by Finite Element and Incremental Harmonic Balance Method, *Nonlinear Dynamics*, 26, (2001) 87-104.

[44] A.H. Nayfeh, *Introduction to Perturbation Techniques*, Wiley, New York, (1981).